

FUTURE INSTABILITY OF FLRW FLUID SOLUTIONS FOR LINEAR EQUATIONS OF STATE $p = K\rho$ WITH $1/3 < K < 1$

FLORIAN BEYER, ELLIOT MARSHALL, AND TODD A. OLIYNYK

ABSTRACT. Using numerical methods, we examine the dynamics of nonlinear perturbations in the expanding time direction, under a Gowdy symmetry assumption, of FLRW fluid solutions to the Einstein-Euler equations with a positive cosmological constant $\Lambda > 0$ and a linear equation of state $p = K\rho$ for the parameter values $1/3 < K < 1$. This paper builds upon the numerical work in [24] in which the simpler case of a fluid on a fixed FLRW background spacetime was studied. The numerical results presented here confirm that the instabilities observed in [24] are also present when coupling to gravity is included as was previously conjectured in [30, 36]. In particular, for the full parameter range $1/3 < K < 1$, we find that the density contrast of the nonlinear perturbations develop steep gradients near a finite number of spatial points and becomes unbounded there at future timelike infinity. This instability is of particular interest since it is not consistent with the standard picture for late time expansion in cosmology.

1. INTRODUCTION

Beginning with the seminal work of Friedrich [10], the future (i.e. expanding) stability of cosmological solutions on exponentially expanding spacetimes has been the source of much research. Recently, on account of their importance in modern standard cosmology [25], the future stability of fluid filled cosmologies with linear equations of state, $p = K\rho$, have been intensively studied with the first rigorous results due to Rodniaski and Speck [33, 35] who proved the future stability of nonlinear perturbations of FLRW (i.e. spatially homogeneous and isotropic) solutions to the Einstein-Euler equations with a positive cosmological constant for the parameter range $0 < K < 1/3$. Stability results for the end points $K = 1/3$ and $K = 0$ were subsequently established in [23] and [15], respectively. Related works have also examined different approaches to establishing stability [11, 20, 21, 26], fluids with nonlinear equations of state [19, 22], and other expanding spacetimes (such as power-law expansion) [9, 31, 36, 37]. All of these results support the standard model of cosmology where $K = 0$ or $K = 1/3$ are the most prominent choices according to which the models are supposed to be near FLRW globally.

Conversely, the question of stability for $1/3 < K < 1$, until recently, remained an open question. In fact, it was widely expected that solutions to the Einstein-Euler equations were unstable when $K > 1/3$. This was primarily a result of the influential work of Rendall [30] who used formal expansions about future timelike infinity to investigate the asymptotic behaviour of relativistic fluids on exponentially expanding FLRW spacetimes. In particular, Rendall found that if $1/3 < K < 1$ and the leading order term in the expansion of the fluid's spatial velocity about timelike infinity vanished at any spatial point, then the formal expansions would become inconsistent. He speculated this was due to inhomogeneous features, so-called spikes, developing in the fluid density which would cause the density contrast to blow-up at future timelike infinity. Another argument supporting the instability of solutions for $1/3 < K < 1$ was given by Speck [36, §1.2.3] who identified certain terms in the equations that might dynamically drive the instability. In any case, this anticipated behaviour for this range of K would not be consistent with the standard picture for late time expansion in which the density contrast remains bounded at late times.

However, more recently the work of the third author [28] proved the existence of a class of non-isotropic spatially homogeneous solutions to the relativistic Euler equations on fixed exponentially expanding FLRW background spacetimes that are (i) stable to the future under small nonlinear perturbations for $1/3 < K < 1/2$ and for which (ii) the initial data of the perturbations could be chosen arbitrarily close to the initial data of a spatially homogeneous and isotropic solution. While the second point implies that the solutions from [28] can be viewed as perturbations of spatially homogeneous and isotropic solutions with zero spatial velocity, it should be noted that the spatial velocity of the fluids in [28] must be non-vanishing everywhere and hence do not constitute a general class of perturbations of spatially homogeneous and isotropic solutions.

In the article [24] by the last two authors, the stability result of [28] was improved to cover the whole parameter range $1/3 < K < 1$. Additionally, a numerical investigation of the stability to the future of the class of spatially homogeneous and isotropic solutions to the Euler equations on fixed FLRW vacuum solutions with positive cosmological constant was carried out. Specifically, numerical solutions of the relativistic Euler equations under a T^2 -symmetry assumption were constructed globally to the future for a class of initial data that included perturbations of spatially homogeneous and isotropic initial data and data for which the spatial

velocity of the fluid vanished at a finite number of points on the initial hypersurface. It is important to emphasize that the vanishing of the fluid's spatial velocity means that these solutions do not satisfy the conditions of the stability theorem from [24].

The main conclusions from the numerical study carried out in [24] can be summarised as follows:

- (1) For each $K \in (1/3, 1)$ and each choice of initial data sufficiently close to spatially homogeneous and isotropic data, the numerical solutions of the relativistic Euler equations display ODE behaviour at late times and are remarkably well-approximated, by an *asymptotic system* that is constructed by discarding all spatial derivatives from a particular formulation of the relativistic Euler equations; see [24, §3.2.2] for details.
- (2) For each $K \in (1/3, 1)$ and each choice of initial data that is sufficiently close to spatially homogeneous initial data and for which the spatial velocity of the fluid vanishes initially at a finite number of points, the density contrast of the fluid develops steep gradients near a finite number of spatial points where it becomes unbounded at future timelike infinity; see [24, §3.2.3] for details.

The aim of the current article is to extend the numerical study of the \mathbb{T}^2 -symmetric relativistic Euler equations from [24] to include coupling to Einstein gravity in the case $1/3 < K < 1$ and thereby to verify quantitatively the conjectures regarding unstable dynamics in [30, 36]. In order to accomplish this, we numerically evolve the Einstein-Euler equations with spatial \mathbb{T}^3 -topology under a Gowdy symmetry assumption (see Section 2.1). The Gowdy spacetimes we consider in this article are especially well-suited to both analytical and numerical treatments (e.g. [1, 2, 3, 4, 5, 6, 7, 8, 16, 17, 18, 29, 32]) due to the presence of two Killing fields, which reduces the Einstein-Euler equations to a 1 + 1-dimensional problem with periodic boundary conditions.

The article is organized as follows: the derivation of a first order formulation of the Gowdy symmetric Einstein-Euler equations that is suitable for numerical implementation and constructing solutions globally to the future is carried out in Section 2. In Section 3, we derive the FLRW background solution which we perturb. Finally, in Section 4, we discuss our numerical setup and results.

2. EINSTEIN-EULER EQUATIONS

2.1. Einstein-Euler equations with Gowdy symmetry. The Einstein-Euler equations¹ for a perfect fluid with a positive cosmological constant are given by

$$G_{ij} + \Lambda g_{ij} = T_{ij}, \quad \Lambda > 0, \quad (2.1)$$

$$\nabla^i T_{ij} = 0, \quad (2.2)$$

where

$$T_{ij} = (\rho + p)v_i v_j + p g_{ij} \quad (2.3)$$

is the stress-energy tensor of a perfect fluid, v_i is the fluid four-velocity normalised by $g^{ij}v_i v_j = -1$, and we assume that the fluid's proper energy density, ρ , and pressure, p , are related via the linear equation of state

$$p = K\rho.$$

Here, the constant K is the square of the sound speed and in order to ensure that the speed of sound is less than or equal to the speed of light, we will always assume that $0 \leq K \leq 1$.

As discussed in the introduction, we restrict our attention to solutions of the Einstein-Euler equations with a Gowdy symmetry [8, 13]. We do this by considering Gowdy metrics in areal coordinates on $\mathbb{R}_{>0} \times \mathbb{T}^3$ that are of the form

$$g_{ij} = e^{2\bar{\eta} - \bar{U}} (-\bar{\alpha} dt \otimes dt + d\theta \otimes d\theta) + e^{2\bar{U}} (dy + Adz)^2 + e^{-2\bar{U}} t^2 dz \otimes dz, \quad (2.4)$$

where the functions $\bar{\eta}$, \bar{U} , $\bar{\alpha}$, and A depend only on $(t, \theta) \in \mathbb{R}_{>0} \times \mathbb{T}$. Here, we take θ to be a periodic coordinate on the 1-torus \mathbb{T} obtained by identifying the ends of the interval $[0, 2\pi]$. In practice, this means that θ is a Cartesian coordinate on \mathbb{R} and that the functions $\bar{\eta}$, \bar{U} , $\bar{\alpha}$, and A are all 2π -periodic in θ . Moreover, as we are only interested in solutions in the expanding direction, i.e. towards the future, we will only concern ourselves with time intervals of the form $t \in [t_0, \infty)$ for some $t_0 > 0$.

In order to facilitate the numerical construction of solutions near timelike infinity, we first transform the metric variables via

$$\bar{\alpha} = \frac{e^{2\alpha}}{4t^3}, \quad \bar{U} = U + \frac{1}{2} \log(t) \quad \text{and} \quad \bar{\eta} = \eta + \log(t),$$

which allows us to express the Gowdy metric (2.4) as

$$g = t \left(e^{2(\eta - U)} \left(-\frac{e^{2\bar{\alpha}}}{4t^3} dt \otimes dt + d\theta \otimes d\theta \right) + e^{2U} (dy + Adz)^2 + e^{-2U} dz \otimes dz \right). \quad (2.5)$$

¹Our indexing conventions are as follows: lower case Latin letters, e.g. i, j, k , will label spacetime coordinate indices that run from 0 to 3 while upper case Latin letters, e.g. I, J, K , will label spatial coordinate indices that run from 1 to 3.

To proceed, we compactify the time interval from $[1, \infty)$ to $(0, 1]$ using the change of time coordinate

$$t = \frac{1}{\tau^2},$$

which, after substituting into (2.5), yields

$$g = \frac{1}{\tau^2} (e^{2(\eta-U)} (-e^{2\alpha} d\tau \otimes d\tau + d\theta \otimes d\theta) + e^{2U} (dy + Adz)^2 + e^{-2U} dz \otimes dz) \quad (2.6)$$

where now $\tau \in (0, 1]$ and the functions η, U, α , and A depend on (τ, θ) and are 2π -periodic in θ . It should be noted that, due to our conventions, future timelike infinity is located at $\tau = 0$ in the direction of *decreasing* τ . As a result, we require $v^0 < 0$ to ensure that the four-velocity v^μ is future oriented with respect to the original time orientation.

Next, we turn to expressing the Einstein-Euler system (2.1)-(2.2) in a Gowdy-symmetric form suitable for numerical implementation. To do so, we express the Einstein equations as a first order system and choose appropriate variables to formulate the Euler equations. The details of the derivation are presented in the following two sections.

2.2. A first order formulation of the Einstein equations. In Gowdy symmetry, the fluid four-velocity only has two non-zero components² and can be expressed as

$$v = v_0 d\tau + v_1 d\theta. \quad (2.7)$$

Using this, we find after a short calculation that the non-zero components of the stress-energy tensor are given by

$$\begin{aligned} T_{00} &= (K+1)\rho(v_0)^2 - \frac{K\rho e^{2\eta-2U+2\alpha}}{\tau^2}, & T_{01} &= (K+1)\rho v_0 v_1, \\ T_{11} &= (K+1)\rho(v_1)^2 + \frac{K\rho e^{2(\eta-U)}}{\tau^2}, & T_{22} &= \frac{K\rho e^{2U}}{\tau^2}, \\ T_{23} &= \frac{K\rho A e^{2U}}{\tau^2}, & T_{33} &= \frac{K\rho(e^{2U} A^2 + e^{-2U})}{\tau^2}. \end{aligned} \quad (2.8)$$

With the help of these expressions and the Gowdy metric (2.6), a straightforward calculation shows that the Einstein equations (2.1) in Gowdy symmetry take the form of three wave equations

$$\begin{aligned} \partial_{\tau\tau} A &= \frac{1}{\tau} e^{-4U} (-2e^{2\eta+2\alpha} A \tau T_{22} + 2e^{2\eta+2\alpha} \tau T_{23} + 4e^{4U+2\alpha} \tau \partial_\theta A \partial_\theta U + e^{4U+2\alpha} \tau \partial_\theta A \partial_\theta \alpha \\ &\quad + e^{4U+2\alpha} \tau \partial_{\theta\theta} A + 2e^{4U} \partial_\tau A - 4e^{4U} \tau \partial_\tau A \partial_\tau U + e^{4U} \tau \partial_\tau A \partial_\tau \alpha) \end{aligned} \quad (2.9)$$

$$\begin{aligned} \partial_{\tau\tau} U &= \frac{-1}{2\tau} e^{-4U} (-e^{2\eta+2\alpha} \tau T_{22} + e^{4U+2\eta+2\alpha} A^2 \tau T_{22} - 2e^{4U+2\eta+2\alpha} A \tau T_{23} + e^{4U+2\eta+2\alpha} \tau T_{33} + e^{8U+2\alpha} \tau (\partial_\theta A)^2 \\ &\quad - 2e^{4U+2\alpha} \tau \partial_\theta U \partial_\theta \alpha - 2e^{4U+2\alpha} \tau \partial_{\theta\theta} U - e^{8U} \tau (\partial_\tau A)^2 - 4e^{4U} \partial_\tau U - 2e^{4U} \tau \partial_\tau U \partial_\tau \alpha) \end{aligned} \quad (2.10)$$

$$\begin{aligned} \partial_{\tau\tau} \eta &= \frac{e^{-2U}}{4\tau^2} (-12e^{2U} + 4e^{2\eta+2\alpha} \Lambda - 4e^{2U+2\eta+2\alpha} A^2 \tau^2 T_{22} + 8e^{2U+2\eta+2\alpha} A \tau^2 T_{23} - 4e^{2U+2\eta+2\alpha} \tau^2 T_{33} \\ &\quad - e^{6U+2\alpha} \tau^2 (\partial_\theta A)^2 + 4e^{2U+2\alpha} \tau^2 (\partial_\theta U)^2 + 4e^{2U+2\alpha} \tau^2 \partial_\theta \eta \partial_\theta \alpha + 4e^{2U+2\alpha} \tau^2 (\partial_\theta \alpha)^2 + 4e^{2U+2\alpha} \tau^2 \partial_{\theta\theta} \eta \\ &\quad + 4e^{2U+2\alpha} \tau^2 \partial_{\theta\theta} \alpha + e^{6U} \tau^2 (\partial_\tau A)^2 + 8e^{2U} \tau \partial_\tau U - 4e^{2U} \tau^2 (\partial_\tau U)^2 - 8e^{2U} \tau \partial_\tau \alpha + 4e^{2U} \tau^2 \partial_\tau \eta \partial_\tau \alpha) \end{aligned} \quad (2.11)$$

and three first order equations

$$\partial_\tau \alpha = \frac{-1}{2\tau} e^{-2U} (6e^{2U} - 2e^{2\eta+2\alpha} \Lambda - e^{2U} \tau^2 T_{00} + e^{2U+2\alpha} \tau^2 T_{11}), \quad (2.12)$$

$$\begin{aligned} \partial_\tau \eta &= \frac{-e^{-2U}}{8\tau} (-12e^{2U} + 4e^{2\eta+2\alpha} \Lambda + 4e^{2U} \tau^2 T_{00} + e^{6U+2\alpha} \tau^2 (\partial_\theta A)^2 + 4e^{2U+2\alpha} \tau^2 (\partial_\theta U)^2 \\ &\quad + e^{6U} \tau^2 (\partial_\tau A)^2 - 8e^{2U} \tau \partial_\tau U + 4e^{2U} \tau^2 (\partial_\tau U)^2), \end{aligned} \quad (2.13)$$

$$\partial_\theta \eta = \frac{1}{4} (-2\tau T_{01} + 4\partial_\theta U - 4\partial_\theta \alpha - e^{4U} \tau \partial_\theta A \partial_\tau A - 4\tau \partial_\theta U \partial_\tau U). \quad (2.14)$$

In particular, (2.13) and (2.14) are the Hamiltonian and momentum constraints, respectively.

In practice, either (2.11) or (2.13) can be used as an evolution equations for η , however only one is needed for our numerical scheme. In this article, we use (2.13). This has the benefit of enforcing the Hamiltonian constraint at every time step and it does not require solving a second order equations for η . Moreover, because

²This follows from choosing coordinates where the two Killing vectors are given by ∂_y and ∂_z , see [18].

we use (2.13) to evolve η , we can view (2.11) as a constraint equation that can be used to verify our numerical results.

Next, introducing the first order variables

$$A_0 = \partial_\tau A, \quad A_1 = e^\alpha \partial_\theta A, \quad U_0 = \partial_\tau U, \quad U_1 = e^\alpha \partial_\theta U, \quad (2.15)$$

we can, with the help of (2.8), express the wave equations (2.9)-(2.10) for A and U in first order form as

$$\partial_\tau \begin{pmatrix} A_0 \\ A_1 \end{pmatrix} + \begin{pmatrix} 0 & -e^\alpha \\ -e^\alpha & 0 \end{pmatrix} \partial_\theta \begin{pmatrix} A_0 \\ A_1 \end{pmatrix} - \alpha_0 \begin{pmatrix} A_0 \\ A_1 \end{pmatrix} = \begin{pmatrix} \frac{1}{\tau}(4\tau A_1 U_1 + 2A_0 - 4\tau A_0 U_0) \\ 0 \end{pmatrix}, \quad (2.16)$$

$$\partial_\tau \begin{pmatrix} U_0 \\ U_1 \end{pmatrix} + \begin{pmatrix} 0 & -e^\alpha \\ -e^\alpha & 0 \end{pmatrix} \partial_\theta \begin{pmatrix} U_0 \\ U_1 \end{pmatrix} - \alpha_0 \begin{pmatrix} U_0 \\ U_1 \end{pmatrix} = \begin{pmatrix} \frac{-1}{2\tau}(e^{4U}\tau A_1^2 - e^{4U}\tau(A_0)^2 - 4U_0) \\ 0 \end{pmatrix}, \quad (2.17)$$

while the remaining Einstein equations are given by

$$\alpha_0 := \partial_\tau \alpha = \frac{-e^{-2U}}{2\tau}(6e^{2U} - 2e^{2\eta+2\alpha}\Lambda + e^{2U}\tau^2(K+1)\rho(v_1^2 e^{2\alpha} - v_0^2) + 2K\rho e^{2(\eta+\alpha)}), \quad (2.18)$$

$$\partial_\tau \eta = \frac{-1}{8\tau} \left(-12 + 4e^{2(\eta+\alpha-U)}(\Lambda - K\rho) + \tau \left(e^{4U}\tau(A_1^2 + A_0^2) - 8U_0 + 4\tau \left((1+K)\rho v_0^2 + U_1^2 + U_0^2 \right) \right) \right), \quad (2.19)$$

$$\begin{aligned} \partial_{\tau\tau}\eta &= \frac{1}{4}e^{4U}(A_0^2 - A_1^2) + \frac{(\Lambda - K\rho)e^{2(\alpha-U+\eta)} + \tau U_0(2 - \tau U_0) + \tau\alpha_0(\tau\partial_\tau\eta - 2) - 3}{\tau^2} \\ &\quad + U_1^2 + e^{2\alpha}(\partial_{\theta\theta}\alpha + \partial_\theta\alpha(\partial_\theta\alpha + \partial_\theta\eta) + \partial_{\theta\theta}\eta), \end{aligned} \quad (2.20)$$

$$\partial_\tau A = A_0, \quad (2.21)$$

$$\partial_\tau U = U_0, \quad (2.22)$$

$$\partial_\theta\eta = \frac{1}{4} \left(-2(1+K)\rho v_0 v_1 \tau - 4\partial_\theta\alpha - e^{4U}\tau A_0 \partial_\theta A + \partial_\theta U(4 - 4\tau U_0) \right), \quad (2.23)$$

where (2.20) and (2.23) are constraint equations.

2.3. A first order formulation of the Euler equations. Contracting the Euler equations (2.2) with the fluid four-velocity v^j and the projection operator $L_j^j = \delta_j^j - \frac{v_j}{v_0}\delta_0^j$, respectively, we find with the help of the normalization condition $v_i v^i = -1$ that the Euler equations can be expressed as³

$$A^i \nabla_i \begin{pmatrix} \rho \\ v_K \end{pmatrix} = \begin{pmatrix} 0 \\ 0 \end{pmatrix} \quad (2.24)$$

where the coefficient matrix A^i is given by

$$A^i = \begin{pmatrix} \frac{K}{\rho+p} v^i & K g^{Kl} (\delta_l^i - \frac{v_l}{v_0} g^{i0}) \\ K g^{Jl} (\delta_l^i - \frac{v_l}{v_0} g^{i0}) & (\rho+p) g^{Jl} g^{Ka} (g_{al} - \frac{2}{v_0} v_{(a} \delta_{l)}^0 + \frac{v_l v_a}{(v_0)^2} g^{00}) v^i \end{pmatrix}$$

and $\nabla_i v_K = \partial_i v_K - \Gamma_{iK}^j v_j$.

We now note by (2.7) that in Gowdy symmetry $\nabla_i v_K$ can be expressed as

$$\nabla_i v_K = \partial_i v_K - \frac{1}{2} \left(g^{00} (\partial_K g_{i0} - \partial_0 g_{iK}) v_0 + g^{11} (\partial_i g_{K1} + \partial_K g_{i1} - \partial_1 g_{iK}) v_1 \right), \quad (2.25)$$

and that the normalisation condition $v_i v^i = -1$ is given by

$$g^{00}(v_0)^2 + g^{11}(v_1)^2 = -1,$$

which can be solved for v_0 to obtain

$$v_0 = \sqrt{-g_{00} - g_{00} g^{11} (v_1)^2}. \quad (2.26)$$

Then, with the help of (2.7), (2.25) and (2.26), we find following a straightforward calculation that the Euler equations (2.24) can be written as

$$B^0 \partial_0 V + B^1 \partial_1 V = F, \quad (2.27)$$

where

$$V = \begin{pmatrix} \rho \\ v_1 \end{pmatrix}, \quad B^0 = \begin{pmatrix} \frac{K}{\rho+K\rho} (g_{11} + (v_1)^2) & K v_1 \\ K v_1 & \rho + K\rho \end{pmatrix},$$

³Note this formulation of the Euler equations was first derived in [27].

$$B^1 = \begin{pmatrix} \frac{K}{\rho+K\rho}v_1 & K \\ K & (\rho+K\rho)\frac{v_1}{g_{11}+(v_1)^2} \end{pmatrix},$$

and

$$F = \frac{1}{2}(-v_0) \begin{pmatrix} K(2g^{11}\partial_1 g_{11} - g^{ab}\partial_1 g_{ab})v_1 \\ (\rho+K\rho)\left(\frac{(v_1)^2}{g_{11}+(v_1)^2}g^{11}\partial_1 g_{11} - g^{00}\partial_1 g_{00}\right) \end{pmatrix} + \frac{K}{2} \begin{pmatrix} (v_1)^2 g^{11}\partial_0 g_{11} - (g_{11}+(v_1)^2)g^{IK}\partial_0 g_{IK} \\ 0 \end{pmatrix}.$$

To proceed, we define re-scaled Gowdy fluid variables $(\tilde{\rho}, \tilde{v}_1)$ via

$$v_1 = \tau^{-\mu-1}\tilde{v}_1 \quad (2.28)$$

$$\rho = \tau^{3(1+K)}\tilde{\rho}, \quad (2.29)$$

where $\mu = \frac{3K-1}{1-K}$. The particular powers of τ in the above definitions are chosen to remove the expected leading order behavior in τ . Now, in order to express the Euler equations (2.27) in terms of these new variables, we differentiate (2.28)-(2.29) to obtain the identities

$$\partial_0 \begin{pmatrix} \rho \\ v_1 \end{pmatrix} = P\partial_0 \begin{pmatrix} \tilde{\rho} \\ \tilde{v}_1 \end{pmatrix} + Z,$$

$$\partial_1 \begin{pmatrix} \rho \\ v_1 \end{pmatrix} = P\partial_1 \begin{pmatrix} \tilde{\rho} \\ \tilde{v}_1 \end{pmatrix},$$

where

$$P = \begin{pmatrix} \tau^{3(1+K)} & 0 \\ 0 & \tau^{-\mu-1} \end{pmatrix} \quad \text{and} \quad Z = \begin{pmatrix} 3(1+K)\tilde{\rho}\tau^{2+3K} \\ (-\mu-1)\tilde{v}_1\tau^{-\mu-2} \end{pmatrix}.$$

Using these identities, it is straightforward to verify that the Euler equations (2.27) can be expressed as

$$\tilde{B}^0\partial_0\tilde{V} + \tilde{B}^1\partial_1\tilde{V} = \tilde{F}, \quad (2.30)$$

where the matrices \tilde{B}^i , \tilde{V} , and \tilde{F} are defined⁴ by

$$\tilde{B}^0 = P^T B^0 P, \quad \tilde{B}^1 = P^T B^1 P, \quad \tilde{V} = \begin{pmatrix} \tilde{\rho} \\ \tilde{v}_1 \end{pmatrix} \quad \text{and} \quad \tilde{F} = P^T(F - B^0 Z),$$

respectively.

2.4. The complete evolution system. Combining (2.30) with (2.16), (2.17), (2.18), (2.21), (2.22), and (2.19) yields a closed set of evolution equations that we will solve numerically. These equations can be expressed in matrix form as

$$\begin{pmatrix} \mathbb{I} & 0 & 0 \\ 0 & \mathbb{I} & 0 \\ 0 & 0 & \tilde{B}^0 \end{pmatrix} \partial_\tau \begin{pmatrix} \mathbf{A} \\ \mathbf{U} \\ \tilde{\mathbf{V}} \end{pmatrix} + \begin{pmatrix} \tilde{B}^1 & 0 & 0 \\ 0 & \tilde{B}^1 & 0 \\ 0 & 0 & \tilde{B}^1 \end{pmatrix} \partial_\theta \begin{pmatrix} \mathbf{A} \\ \mathbf{U} \\ \tilde{\mathbf{V}} \end{pmatrix} = \begin{pmatrix} \alpha_0 \mathbb{I} & 0 & 0 \\ 0 & \alpha_0 \mathbb{I} & 0 \\ 0 & 0 & 0 \end{pmatrix} \begin{pmatrix} \mathbf{A} \\ \mathbf{U} \\ \tilde{\mathbf{V}} \end{pmatrix} + \begin{pmatrix} F_A \\ F_U \\ F_{\tilde{V}} \end{pmatrix}, \quad (2.31)$$

$$\partial_\tau \begin{pmatrix} \alpha \\ \eta \\ A \\ U \end{pmatrix} = \begin{pmatrix} F_\alpha \\ F_\eta \\ A_0 \\ U_0 \end{pmatrix}, \quad (2.32)$$

where

$$\mathbf{A} = \begin{pmatrix} A_0 \\ A_1 \end{pmatrix},$$

$$\mathbf{U} = \begin{pmatrix} U_0 \\ U_1 \end{pmatrix},$$

$$\tilde{\mathbf{V}} = \begin{pmatrix} \tilde{\rho} \\ \tilde{v}_1 \end{pmatrix},$$

$$\tilde{B}^1 = \begin{pmatrix} 0 & -e^\alpha \\ -e^\alpha & 0 \end{pmatrix},$$

$$\tilde{B}^0 = \begin{pmatrix} K\tau^{3K+1}(e^{2\eta-2U} + \tilde{v}_1^2\tau^{-2\mu}) & K\tilde{v}_1\tau^{3K-2\mu+1} \\ K\tilde{v}_1\tau^{3K-2\mu+1} & (K+1)\tilde{\rho}\tau^{3K-2\mu+1} \end{pmatrix},$$

$$\tilde{B}^1 = \begin{pmatrix} -\frac{K\tilde{v}_1\tau^{3K-\mu+1}e^\alpha\sqrt{\tilde{v}_1^2\tau^{-2\mu} + e^{2\eta-2U}}}{(K+1)\tilde{\rho}} & -K\tau^{3K-\mu+1}e^\alpha\sqrt{\tilde{v}_1^2\tau^{-2\mu} + e^{2\eta-2U}} \\ -K\tau^{3K-\mu+1}e^\alpha\sqrt{\tilde{v}_1^2\tau^{-2\mu} + e^{2\eta-2U}} & -\frac{e^\alpha(1+K)\tilde{\rho}\tilde{v}_1\tau^{3K-3\mu+1}}{\sqrt{e^{-2U+2\eta} + \tilde{v}_1^2\tau^{-2\mu}}} \end{pmatrix},$$

⁴Here T denotes the transpose of a matrix.

$$\begin{aligned}
F_A &= \begin{pmatrix} \frac{1}{\tau} (4\tau A_1 U_1 + 2A_0 - 4\tau A_0 U_0) \\ 0 \end{pmatrix}, \\
F_U &= \begin{pmatrix} \frac{-1}{2\tau} (e^{4U} \tau A_1^2 - e^{4U} \tau (A_0)^2 - 4U_0) \\ 0 \end{pmatrix}, \\
F_{\tilde{V}} &= \begin{pmatrix} K\tau^{3K+1} e^{2\eta-2U} (U_0 - \partial_\tau \eta) + K\tilde{v}_1 \tau^{3K-\mu+1} e^\alpha \sqrt{e^{2\eta-2U} + \tilde{v}_1^2 \tau^{-2\mu}} \partial_\theta \alpha + K\mu \tilde{v}_1^2 \tau^{3K-2\mu} \\ (K+1)\tilde{\rho} \tau^{3K-2\mu} \left(\frac{\tau^{\mu+1} e^\alpha \sqrt{e^{2\eta-2U} + \tilde{v}_1^2 \tau^{-2\mu}} (\tau^{2\mu} e^{2\eta} (\partial_\theta \alpha - \partial_\theta U + \partial_\theta \eta) + \tilde{v}_1^2 e^{2U} \partial_\theta \alpha)}{\tilde{v}_1^2 e^{2U} + \tau^{2\mu} e^{2\eta}} + \tilde{v}_1 (-3K + \mu + 1) \right) \end{pmatrix}, \\
F_\alpha &= \frac{\left(2\Lambda - (K-1)\tilde{\rho} \tau^{3K+3} \right) e^{2(\alpha-U+\eta)} - 6}{2\tau}, \\
F_\eta &= \frac{1}{8} e^{-2U} \tau^{-1-2\mu} \left(-4e^{2(U+\alpha)} (1+K)\tilde{\rho} \tilde{v}_1^2 \tau^{3+3K} - \tau^{2\mu} \left(4 \left(-3e^{2U} + e^{2(\eta+\alpha)} (\Lambda + \tilde{\rho} \tau^{3+3K}) \right) \right. \right. \\
&\quad \left. \left. + e^{2U} \tau \left(e^{4U} \tau (A_1^2 + A_0^2) - 8\partial_\tau U + 4\tau (U_1^2 + U_0^2) \right) \right) \right).
\end{aligned}$$

Remark 2.1. While the form of the equations (2.31)-(2.32) is suitable for numerical implementation, it is not immediately obvious that the system has a well-posed initial value problem. By re-writing the equations as a symmetric hyperbolic system we can ensure this is the case. The Euler equations prove to be the only impediment to this goal, in particular the derivatives of metric functions in the source term $F_{\tilde{V}}$ necessitate the use of new variables. By slightly modifying the process in [14] and introducing the scalar velocity $v = \frac{v^1}{e^\alpha v^0}$, a new metric variable $\nu = \eta + \alpha$, and a modified density variable $\gamma = e^{\nu-U} \rho$, it is possible to write the Euler equations in the form

$$C^0 \partial_\tau \begin{pmatrix} \gamma \\ v \end{pmatrix} + C^1 \partial_\theta \begin{pmatrix} \gamma \\ v \end{pmatrix} = G \quad (2.33)$$

where G only contains derivatives of U and A which can be expressed in terms of the first order variables defined earlier (2.15). Multiplying (2.33) on the left by $P(C^0)^{-1}$ for an appropriate symmetric matrix P , it is then possible to put the Euler equations in symmetric hyperbolic form. Finally, by replacing all remaining terms in (2.31)-(2.32) with the new variables, the Einstein-Euler equations in Gowdy symmetry can be cast in symmetric hyperbolic form.

3. FLRW SOLUTIONS

Before we can choose appropriate initial data for our numerical scheme, we must first identify the FLRW solutions (i.e. spatially homogeneous and isotropic) that we wish to perturb. Recalling the form of the Gowdy metric (2.6), we observe that a FLRW metric is obtained by setting $U = A = \eta = 0$ and assuming that the remaining metric function α only depends on τ . For the Gowdy fluid variables $\tilde{\rho}$ and \tilde{v}_1 , spatial homogeneity and isotropy requires that $\tilde{v}_1 = 0$ and that $\tilde{\rho}$ also only depends on τ . From these considerations, we conclude via (2.31) and (2.32) that FLRW solutions of the Einstein-Euler equations are obtained from solving

$$\partial_\tau \tilde{\rho} = 0, \quad (3.1)$$

$$\partial_\tau \alpha = \frac{(2\Lambda - (K-1)\tilde{\rho} \tau^{3K+3}) e^{2\alpha} - 6}{2\tau}, \quad (3.2)$$

$$\partial_\tau \eta = 0 = \frac{(\Lambda + \tilde{\rho} \tau^{3K+3}) e^{2\alpha} - 3}{2\tau}. \quad (3.3)$$

Now, by (3.3), we observe that

$$\alpha = \frac{1}{2} \ln \left(\frac{3}{\Lambda + \tilde{\rho} \tau^{3K+3}} \right),$$

which we note automatically satisfies (3.2). Furthermore, we find from (2.29) and (3.1) that

$$\rho = \rho_c \tau^{3(1+K)},$$

where $\rho_c \in \mathbb{R}^+$ is a freely specifiable constant. From this, we deduce that the FLRW solutions of the Einstein-Euler equations are given by

$$\begin{aligned} g &= \frac{1}{\tau^2} \left(-\frac{3}{\Lambda + \rho_c \tau^{3(1+K)}} d\tau^2 + d\theta^2 + dy^2 + dz^2 \right), \\ \rho &= \rho_c \tau^{3(1+K)}, \\ v &= \left(\frac{3}{\Lambda + \rho_c \tau^{3(1+K)}} \right)^{\frac{1}{2}} d\tau. \end{aligned} \tag{3.4}$$

Remark 3.1. Expressing the momentum constraint equations (2.14) in terms of \tilde{v}_1 and $\tilde{\rho}$, we observe that

$$\partial_\theta \eta = -\frac{1}{2}(1+K)\tilde{\rho}\tilde{v}_1\tau^{2+3K-\mu}e^\alpha\sqrt{(e^{2\eta-2U} + \tilde{v}_1^2\tau^{-2\mu})} - \partial_\theta\alpha - \frac{1}{4}e^{4U}\tau A_0\partial_\theta A + \partial_\theta U(1 - \tau U_0). \tag{3.5}$$

Since all spatial derivatives would vanish on a spatially homogeneous, but not necessarily isotropic, solution, it follows from the positivity of the density, i.e. $\tilde{\rho} > 0$ everywhere, that $\tilde{v}_1 = 0$ must be satisfied for all spatially homogeneous solutions. This, in particular, shows that self-gravitating versions of the non-isotropic spatially homogeneous fluid solutions of the type considered in [24], known as *tilted* solutions, are incompatible with Gowdy symmetry. As it turns out, tilted solutions require a non-trivial spatial topology; see [12]. We will report on the nonlinear stability of tilted solutions in a separate article.

4. NUMERICAL RESULTS

4.1. Numerical Setup. In the numerical setup that we use to solve (2.31)-(2.32), the computational spatial domain is $[0, 2\pi]$ with periodic boundary conditions which is discretised using an equidistant grid with N grid points. Spatial derivatives are discretised using 2nd order central finite differences and time integration is performed using a standard 2nd order Runge-Kutta method (*Heun's Method*). As a consequence, our code is second order accurate. We also enforce the CFL condition to ensure convergence. In this case we have used the tightened 4/3 CFL condition for Heun's Method which is discussed in [34].

4.1.1. Initial Data. The choice of initial data is not completely trivial as we must satisfy the Hamiltonian (2.19) and momentum (2.23) constraints initially. The Hamiltonian constraint (2.19) is enforced at every time-step, as we use it as an evolution equation for η . Consequently, we only need to ensure our choice of initial data satisfies the momentum constraint (2.23). Additionally, we must satisfy the constraints (2.15) that arise from the definition of the first order variables A_1 and U_1 . Our choice of initial data (4.1) ensures all these constraints are satisfied initially.

As discussed in the introduction, the main aim of this article is to determine whether the density contrast blows up when the fluid is coupled to the gravitational field in the same way as we observed in the fixed background spacetime case [24]. Hence, we must choose initial data so that the fluid's spatial velocity vanishes somewhere on the domain initially.

For Gowdy symmetry, this amounts to the initial data for \tilde{v}_1 vanishing somewhere on the initial hypersurface. Moreover, since $\tilde{v}_1 = 0$ for the FLRW solutions, we must select initial data so that \tilde{v}_1 is everywhere close to zero on the initial hypersurface in order for it to represent a small perturbation of FLRW initial data. In our numerical simulations, we satisfy these constraints on the initial data for \tilde{v}_1 by using sinusoidal functions with a small amplitude parameter called a below. In particular, our initial data for \tilde{v}_1 crosses zero at least twice on the initial hypersurface, and we note that this initial data is essentially the same as was used in [24].

For the remainder of this article, with the exception of Section 4.1.3, we employ initial data of the form

$$\begin{aligned}
\dot{\tilde{v}}_1 &= a \sin(\theta), \\
\dot{\tilde{\rho}} &= \frac{1}{\frac{1}{2}(1+K)\sqrt{e^{2\dot{\alpha}}(e^{2\dot{\eta}}-2\dot{U} + \dot{v}_1^2)}}, \\
\dot{\alpha} &= a \cos(\theta) + \frac{1}{2} \log\left(\frac{3}{\Lambda + \frac{2}{(1+K)}}\right), \\
\dot{\eta} &= a \sin(\theta), \\
\dot{U} &= a \sin(\theta) + c, \\
\dot{U}_0 &= bd, \\
\dot{U}_1 &= e^{\dot{\alpha}} \partial_\theta \dot{U}, \\
\dot{A} &= de^{-4c-4a \sin(\theta)} + c, \\
\dot{A}_0 &= b, \\
\dot{A}_1 &= e^{\dot{\alpha}} \partial_\theta \dot{A},
\end{aligned} \tag{4.1}$$

where a, b, c, d are constants to be specified. Initial data of this form can be considered a perturbation of FLRW initial data provided that the constants a, b, c and d are chosen sufficiently close to zero. This follows from the fact that setting $a = b = c = d = 0$ in (4.1) produces FLRW initial data. If the size of the parameters a, b, c, d are too large the system is found to become unstable almost immediately. That is, within a small amount of timesteps the variables develop steep gradients and produce numerical errors. Throughout this article we focus exclusively on initial data with small amplitudes. In particular, all the plots in this section have been generated with $a = b = c = d = 0.01$.

4.1.2. *Code Tests.* We have verified the second order accuracy of our code with convergence tests involving perturbations of FLRW solutions using resolutions of $N = 200, 400, 800, 1600, 3200$, and 6400 grid points. To estimate the numerical discretisation error Δ for any of our unknowns, we took the \log_2 of the absolute value of the difference between each simulation and the highest resolution run. The results for \tilde{v}_1 and $\tilde{\rho}$ are shown⁵ in Figures 1(a)-1(b) from which the second order convergence is clear.

As a further check on the accuracy of the code, we can measure how much the constraints are violated

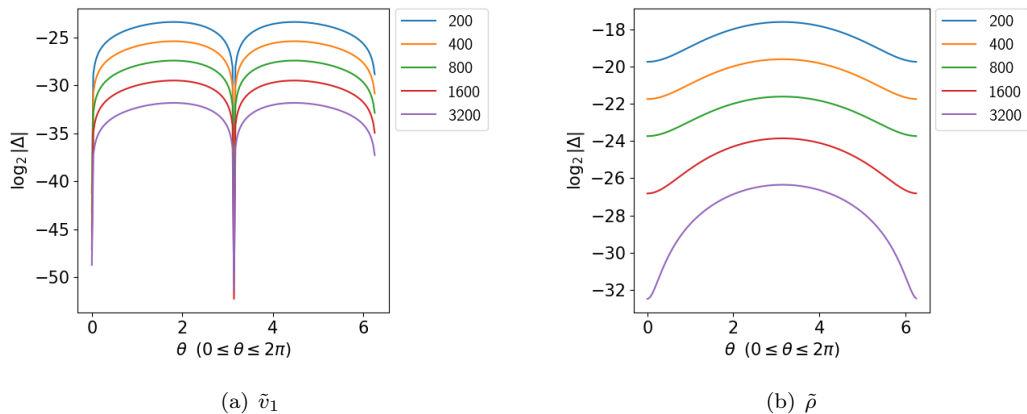


FIGURE 1. Convergence plots of \tilde{v}_1 and $\tilde{\rho}$ at $\tau = 0.599$, $K = 0.5$, $\Lambda = 1$.

during the evolution of the system. Beginning with the momentum constraint (3.5), we define the quantity

$$C_1 = -\partial_\theta \eta - \frac{1}{2}(1+K)\tilde{\rho}\tilde{v}_1\tau^{2+3K-\mu}e^\alpha\sqrt{(e^{2\eta}-2U + \tilde{v}_1^2\tau^{-2\mu})} - \partial_\theta \alpha - \frac{1}{4}e^{4U}\tau A_0\partial_\theta A + \partial_\theta U(1 - \tau U_0). \tag{4.2}$$

Clearly, $C_1 = 0$ means that the momentum constraint is identically satisfied. The quantity $\log_2 \|C_1\|_2$ can therefore be understood as the violation error of the momentum constraint as a function of time. In a similar

⁵It should be noted that we have also performed convergence tests for all other variables and confirmed second order convergence. These plots are omitted here for brevity.

manner, we can also define constraint violation quantities from the definitions of our first order variables A_1 and U_1 , and from the wave equation for η , (2.20), as follows

$$\begin{aligned} C_2 &= A_1 - e^\alpha \partial_\theta A, \\ C_3 &= U_1 - e^\alpha \partial_\theta U, \\ C_4 &= \partial_{\tau\tau}\eta - \left(\frac{1}{4\tau^2} (-12 + 4e^{2(-U+\eta+\alpha)})(\Lambda - K\tilde{\rho}\tau^{3+3K}) + 8\tau(U_0 - \alpha_0) \right. \\ &\quad \left. + \tau^2(4U_1^2 + 4e^{2\alpha}(\partial_\theta\alpha(\partial_\theta\eta + \partial_\theta\alpha) + \partial_{\theta\theta}\eta + \partial_{\theta\theta}\alpha)) + e^{4U}(-A_1^2 + A_0^2) - 4U_0^2 + 4\partial_\tau\eta\partial_\tau\alpha \right). \end{aligned}$$

The time derivatives for C_4 are calculated numerically using a fourth order finite difference stencil for the second derivative

$$(\partial_{\tau\tau}\eta)_{i,j} = \frac{-\eta_{i-2,j} + 16\eta_{i-1,j} - 30\eta_{i,j} + 16\eta_{i+1,j} - \eta_{i+2,j}}{12(\Delta\tau)^2}, \quad (4.3)$$

where $\eta_{i,j}$ denotes the value of η at the i^{th} timestep and j^{th} spatial grid point and $\Delta\tau$ is the timestep size. We observe the expected second order convergence for the quantities $\log_2(\|C_1\|_2 + \|C_2\|_2 + \|C_3\|_2)$ and $\log_2(\|C_4\|_2)$ shown in Figures 2(a) and 2(b) respectively. Even though the constraints are identically satisfied at the initial time by virtue of our choice of initial data (4.1), we note the numerical value is not exactly zero, even at the initial time $\tau = 1$, as the derivatives in C_1 (4.2), C_2 , C_3 , and C_4 are approximated by finite differences. It should also be noted that, due to our use of the stencil (4.3), the first and last two timesteps have been removed from Figure 2(b).

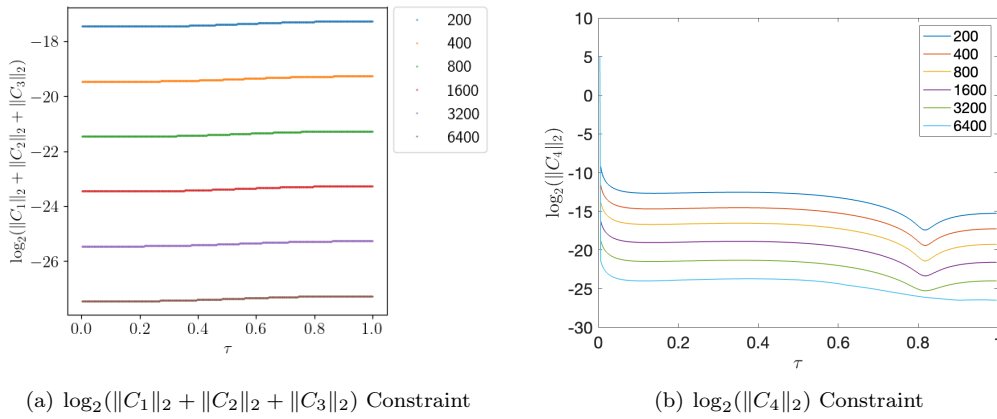


FIGURE 2. Convergence plots of the constraint quantities, $K = 0.5$, $\Lambda = 1$. The system was evolved until $\tau = 0.002$.

4.1.3. *Code Validation.* A simple way to test the validity of our code is to compare our numerical solution with the FLRW solution (3.4). For this convergence test, we employ the following initial data

$$\begin{aligned} \tilde{\rho} &= 1, \\ \alpha &= \frac{1}{2} \log\left(\frac{3}{\Lambda + 1}\right), \\ A &= A_1 = A_0 = U = U_1 = U_0 = \eta = \tilde{v}_1 = 0. \end{aligned}$$

Once again, we observe the expected second order convergence, shown for α and $\tilde{\rho}$ in Figures 3(a) and 3(b), respectively.

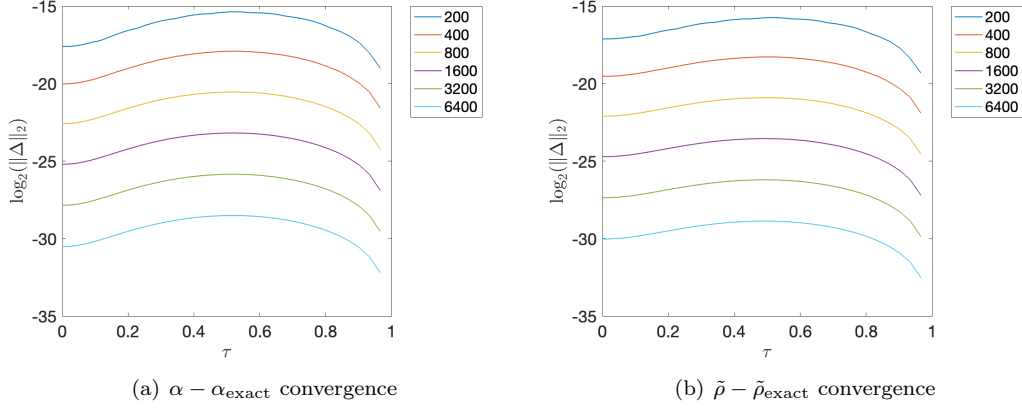


FIGURE 3. Convergence plots of the L_2 norm of $\alpha - \alpha_{\text{exact}}$ and $\tilde{\rho} - \tilde{\rho}_{\text{exact}}$, $K = 0.4$, $\Lambda = 1$. The system was evolved until $\tau = 0.002$.

4.2. Numerical Behaviour. We now examine the behaviour of numerical solutions of (2.31)-(2.32) with initial data of the form (4.1). From our numerical simulations, we observe that the asymptotic behaviour of the fluid variables and the density contrast are broadly consistent with what was observed in [24, §3.2] in the fixed background spacetime case. More specifically, for the full parameter range $1/3 < K < 1$ and all choices of the initial data with a , b , c , and d sufficiently small, we observe that all the gravitational and fluid variables, with the exception of $\tilde{\rho}$, remain bounded. It is unclear from our numerical solutions whether $\tilde{\rho}$ remains bounded at timelike infinity. On the other hand, the spatial derivative of the density, $\partial_\theta \tilde{\rho}$, always develops steep gradients at finitely many points and becomes unbounded as $\tau \searrow 0$ for all $K \in (1/3, 1)$, shown in Figure 4, indicating that the system is unstable.

In turn, this means the density contrast, which is a measure of deviation from spatial homogeneity, also forms steep gradients and becomes unbounded as $\tau \searrow 0$, where we note $\tau = 0$ corresponds to future timelike infinity. We present plots of the density contrast in Section 4.2.2.

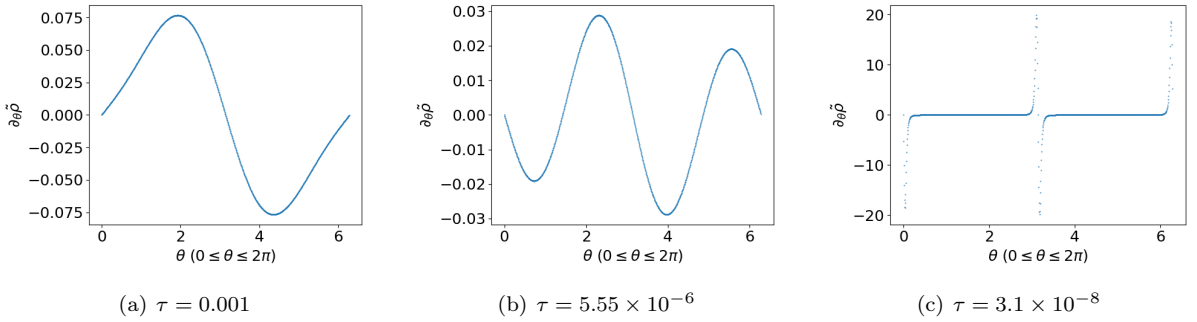


FIGURE 4. Plots of the derivative of the re-scaled density, $\partial_\theta \tilde{\rho}$, at various times. $N = 1000$, $K = 0.5$, $\Lambda = 1$.

4.2.1. Asymptotic Behaviour and Approximations. In [24, §3.2], it was observed that the fluid variables displayed ODE-like behaviour at late times. This can also be seen for the metric and fluid variables in our simulations. In particular, we observe that, near $\tau = 0$, solutions to the Gowdy-Euler equations are remarkably well approximated by solutions to the asymptotic system

$$\partial_\tau A_0 = \alpha_0 A_0 + \frac{1}{\tau} (4\tau A_1 U_1 + 2A_0 - 4\tau A_0 U_0), \quad (4.4)$$

$$\partial_\tau A_1 = \alpha_0 A_1, \quad (4.5)$$

$$\partial_\tau U_0 = \alpha_0 U_0 - \frac{1}{2\tau} (e^{4U} \tau A_1^2 - e^{4U} \tau A_0^2 - 4U_0), \quad (4.6)$$

$$\partial_\tau U_1 = \alpha_0 U_1, \quad (4.7)$$

$$\partial_\tau \tilde{\rho} = \frac{1}{-e^{2U} (-1 + K) \tilde{v}_1^2 + e^{2\eta} \tau^{2\mu}} \left(\tau^{-1} (1 + K) \tilde{\rho} \left(e^{2U} (-1 + 3K) \tilde{v}_1^2 \right. \right.$$

$$+ e^{2\eta}\tau^{1+2\mu}(U_0 - \partial_\tau\eta) + \frac{e^{2\eta}\tilde{v}_1\tau^{\mu+1}U_1}{\sqrt{e^{2(\eta-U)} + \tilde{v}_1^2\tau^{-2\mu}}}\Bigg), \quad (4.8)$$

$$\partial_\tau\tilde{v}_1 = \frac{1}{\tau(\tau^{2\mu}e^{2\eta} - (K-1)\tilde{v}_1^2e^{2U})}\left(e^{-\alpha}\left(\tilde{v}_1\tau^{2\mu}e^{\alpha+2\eta}(K\tau(\partial_\tau\eta - U_0) - 3K + \mu + 1)\right.\right. \\ \left.\left.- \tilde{v}_1^3(K(\mu+3) - \mu - 1)e^{\alpha+2U} - U_1\tau^{3\mu+1}e^{2\eta+\alpha}\sqrt{(e^{2\eta-2U} + \tilde{v}_1^2\tau^{-2\mu})}\right)\right), \quad (4.9)$$

$$\partial_\tau\alpha = \frac{(2\Lambda - (K-1)\tilde{\rho}\tau^{3K+3})e^{2(\alpha-U+\eta)} - 6}{2\tau}, \quad (4.10)$$

$$\partial_\tau\eta = \frac{1}{8}e^{-2U}\tau^{-1-2\mu}\left(-4e^{2(U+\alpha)}(1+K)\tilde{\rho}\tilde{v}_1^2\tau^{3+3K} - \tau^{2\mu}\left(4\left(-3e^{2U} + e^{2(\eta+\alpha)}(\Lambda + \tilde{\rho}\tau^{3+3K})\right)\right.\right. \\ \left.\left.+ e^{2U}\tau\left(e^{4U}\tau(A_1^2 + A_0^2) - 8\partial_\tau U + 4\tau(U_1^2 + U_0^2)\right)\right)\right), \quad (4.11)$$

$$\partial_\tau A = A_0, \quad (4.12)$$

$$\partial_\tau U = U_0. \quad (4.13)$$

This system is obtained by setting the spatial derivative terms in (2.31)-(2.32) to zero. We have tested the agreement between solutions of the full Einstein-Euler equations (2.31)-(2.32) and the asymptotic system (4.4)-(4.13) using the following procedure, which is similar to the one employed in [24, §3.2.2]:

- (i) Generate a numerical solution $(A, A_1, A_0, U, U_1, U_0, \alpha, \eta, \tilde{\rho}, \tilde{v}_1)$ of the Einstein-Euler equations (2.31)-(2.32) from initial data specified at $\tau_0 > 0$.
- (ii) Fix a time⁶ $\tilde{\tau}_0$ when the solution from step (i) appears to be first dominated by ODE behaviour.
- (iii) Fix initial data for the asymptotic system (4.4)-(4.13) at $\tau = \tilde{\tau}_0$ by setting

$$(\bar{A}_I, \bar{A}_{1,I}, \bar{A}_{0,I}, \bar{U}_I, \bar{U}_{1,I}, \bar{U}_{0,I}, \bar{\alpha}_I, \bar{\eta}_I, \bar{\rho}_I, \bar{v}_{1,I}) = (A, A_1, A_0, U, U_1, U_0, \alpha, \eta, \tilde{\rho}, \tilde{v}_1)|_{\tilde{\tau}_0}.$$

- (iv) Numerically solve the asymptotic system (4.4)-(4.13) using the initial data from (iii) to obtain a solution $(\bar{A}, \bar{A}_1, \bar{A}_0, \bar{U}, \bar{U}_1, \bar{U}_0, \bar{\alpha}, \bar{\eta}, \bar{\rho}, \bar{v}_1)$.
- (v) Compare the solutions $(\bar{A}, \bar{A}_1, \bar{A}_0, \bar{U}, \bar{U}_1, \bar{U}_0, \bar{\alpha}, \bar{\eta}, \bar{\rho}, \bar{v}_1)$ and $(A, A_1, A_0, U, U_1, U_0, \alpha, \eta, \tilde{\rho}, \tilde{v}_1)$ on the region $(0, \tilde{\tau}_0)$.

Following this process, we observe that the metric variables A, U, A_1, U_1, α , and η become effectively constant for $\tau \in (0, \tilde{\tau}_0)$ and are indistinguishable from the corresponding asymptotic solution $\bar{A}, \bar{U}, \bar{A}_1, \bar{U}_1, \bar{\alpha}$, and $\bar{\eta}$, while the variables A_0, U_0, \bar{A}_0 , and \bar{U}_0 all rapidly decay to zero. On the other hand, the fluid variables, \tilde{v}_1 and $\tilde{\rho}$, display significantly more dynamic, but still ODE-dominated, behaviour before converging to fixed functions for $\tau \in (0, \tilde{\tau}_0)$. In particular, the fluid variables closely match their asymptotic counterparts, shown for \tilde{v}_1 in Figure 5. Furthermore, we note that \tilde{v}_1 and \bar{v}_1 show strong agreement even at the locations where spike points form in the density contrast, cf. Figure 6.

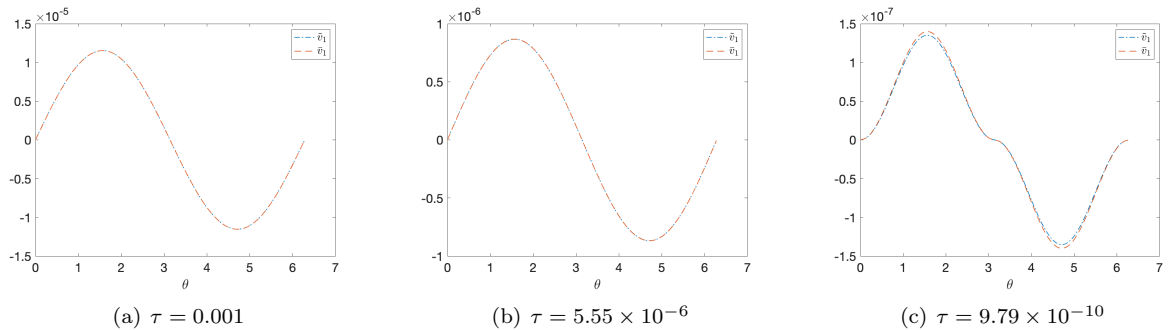


FIGURE 5. Comparison of full Einstein-Euler solution \tilde{v}_1 (in blue) and asymptotic solution \bar{v}_1 (in orange) at various times. $\tilde{\tau}_0 = 0.001$, $N = 1000$, $K = 0.5$, $\Lambda = 1$.

⁶It is worth noting that the value of $\tilde{\tau}_0$ decreases as $K \nearrow 1$.

4.2.2. *Behaviour of the Density Contrast.* The density contrast is, by definition, $\frac{\partial_{\theta}\rho}{\rho}$. In terms of the re-scaled density (2.29), it is given by

$$\frac{\partial_{\theta}\rho}{\rho} = \frac{\partial_{\theta}\tilde{\rho}}{\tilde{\rho}}.$$

Using this relation, we observe from the numerical simulations that the density contrast develops steep gradients and blows-up at $\tau = 0$ at isolated spatial points, shown in Figure 6. As discussed in the introduction, this behaviour was anticipated by Rendall in [30] and it notable because the blow-up of the density contrast at timelike infinity is incompatible with the standard picture of late time expansion in cosmology in which the density contrast is zero for FLRW solutions. The density contrast blow-up at timelike infinity also indicates an

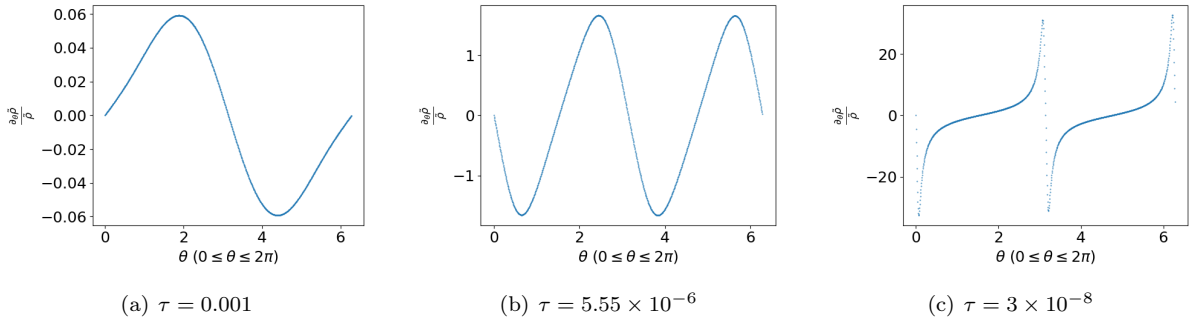


FIGURE 6. Density contrast $\frac{\partial_{\theta}\rho}{\rho}$ at various times. $N = 1000$, $K = 0.5$, $\Lambda = 1$.

instability in the sense that density contrast of the perturbed solutions does not remain uniformly bounded no matter how close the initial data is chosen to FLRW initial data. It should be noted, however, that the blow-up of the density contrast is more apparent as the size of K increases. In particular, for values of K close to $1/3$ one needs to choose initial data with larger values of a , b , c , and d to observe the blow-up within the timespan of our numerical evolutions.

Finally, as in Section 4.2.1, we can compare the density contrast computed from solutions of the full Einstein-Euler equations (2.31)-(2.32) with the the density contrast generated from the asymptotic system. Once again the full Einstein-Euler and asymptotic plots are almost indistinguishable, shown in Figure 7.

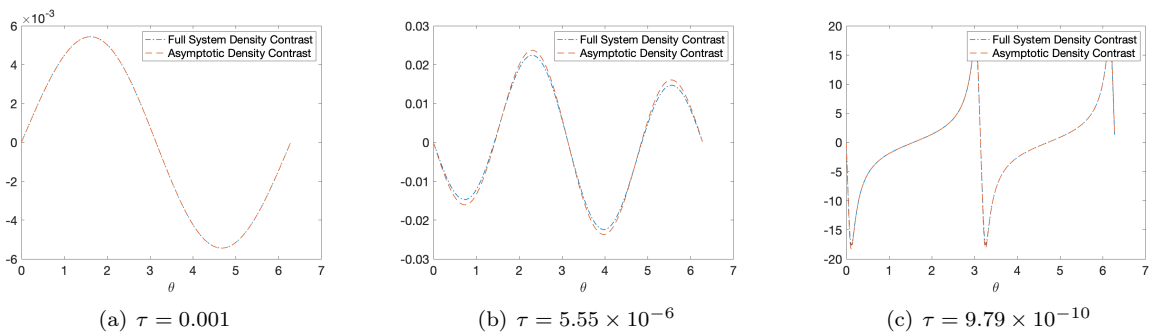


FIGURE 7. Comparison between the full Einstein-Euler (in blue) and asymptotic density contrast (in orange) at various times. $\tilde{\tau}_0 = 0.001$, $N = 1000$, $K = 0.5$, $\Lambda = 1$.

5. DISCUSSION

The aim of this work was to numerically study nonlinear perturbations of FLRW solutions to the Einstein-Euler equations under a Gowdy symmetry assumption and linear equation of state $p = K\rho$ for $K \in (1/3, 1)$. In particular, we wished to determine whether the blow-up of the density contrast $\frac{\partial_{\theta}\rho}{\rho}$ at isolated spatial points at timelike infinity, anticipated by Rendall [30] and subsequently numerically observed for the relativistic Euler equations on an exponentially expanding FLRW spacetime in [24], also occurs when coupling to Einstein gravity is included. We have numerically solved the Einstein-Euler equations using a standard second-order Runge-Kutta method in time and second-order central finite differences to discretise spatial derivatives. The expected second order accuracy of this implementation was confirmed by our convergence tests. Using this

numerical scheme, we have found that the density contrast blows up at finitely many spatial points as $\tau \searrow 0$ for all $K \in (1/3, 1)$ and all choices of initial data that is sufficiently close to FLRW initial data and for which \tilde{v}_1 crosses zero somewhere on the initial hypersurface. These results are consistent with the density contrast blow-up scenario put forth by Rendall. This instability is particularly notable as it is incompatible with the standard picture of late time expansion in cosmology. We have also observed that, for initial data suitably close to spatially homogeneous initial data, solutions display ODE-like behaviour at late times analogous to the behaviour found in [24].

There are several directions for future research to take. An obvious next step would be to remove the Gowdy symmetry assumption and study the full 3+1 system. Additionally, while we believe the initial data we have studied is reasonably ‘generic’, it would be interesting to test a wider variety of initial conditions to see what, if any, impact this has on the behaviour of solutions.

REFERENCES

1. E. Ames, F. Beyer, J. Isenberg, and P. G. LeFloch, *A class of solutions to the Einstein equations with AVTD behavior in generalized wave gauges*, J. Geom. Phys. **121** (2017), 42–71.
2. Paulo Amorim, Christine Bernardi, and Philippe G. LeFloch, *Computing Gowdy spacetimes via spectral evolution in future and past directions*, Classical and Quantum Gravity **26** (2009), no. 2, 025007, DOI: [10.1088/0264-9381/26/2/025007](https://doi.org/10.1088/0264-9381/26/2/025007).
3. Beverly K Berger and Vincent Moncrief, *Numerical investigation of cosmological singularities*, Physical Review D **48** (1993), no. 10, 4676–4687, DOI: [10.1103/PhysRevD.48.4676](https://doi.org/10.1103/PhysRevD.48.4676).
4. F. Beyer and J. Hennig, *Smooth Gowdy-symmetric generalized Taub-Nut solutions*, Classical and Quantum Gravity **29** (2012), no. 24, 245017.
5. F. Beyer and P. G. LeFloch, *Second-order hyperbolic Fuchsian systems and applications*, Class. Quantum Grav. **27** (2010), no. 24, 245012.
6. ———, *Self-gravitating fluid flows with Gowdy symmetry near cosmological singularities*, Commun. Part. Diff. Eq. **42** (2017), no. 8, 1199–1248.
7. Florian Beyer and Philippe G. LeFloch, *A numerical algorithm for Fuchsian equations and fluid flows on cosmological spacetimes*, Journal of Computational Physics **431** (2021), 110145, DOI: [10.1016/j.jcp.2021.110145](https://doi.org/10.1016/j.jcp.2021.110145).
8. Piotr T Chruściel, *On space-times with $U(1) \times U(1)$ symmetric compact Cauchy surfaces*, Annals of Physics **202** (1990), no. 1, 100–150, DOI: [10.1016/0003-4916\(90\)90341-K](https://doi.org/10.1016/0003-4916(90)90341-K).
9. D. Fajman, T.A. Oliynyk, and Zoe Wyatt, *Stabilizing relativistic fluids on spacetimes with non-accelerated expansion*, Commun. Math. Phys. **383** (2021), 401–426.
10. H. Friedrich, *On the existence of n -geodesically complete or future complete solutions of Einstein’s field equations with smooth asymptotic structure*, Commun. Math. Phys. **107** (1986), 587–609.
11. ———, *Sharp asymptotics for Einstein- λ -dust flows*, Comm. Math. Phys. **350** (2017), 803 – 844.
12. M. Goliath and G.F.R. Ellis, *Homogeneous cosmologies with a cosmological constant*, Phys. Rev. D **60** (1999), 023502.
13. Robert H Gowdy, *Vacuum spacetimes with two-parameter spacelike isometry groups and compact invariant hypersurfaces: Topologies and boundary conditions*, Annals of Physics **83** (1974), no. 1, 203–241, DOI: [10.1016/0003-4916\(74\)90384-4](https://doi.org/10.1016/0003-4916(74)90384-4).
14. N. Grubic and P.G. LeFloch, *Weakly regular Einstein–Euler spacetimes with Gowdy symmetry: The global areal foliation*, Arch. Rat. Mech. **208** (2013), no. 2, 391–428.
15. M. Hadžić and J. Speck, *The global future stability of the FLRW solutions to the Dust–Einstein system with a positive cosmological constant*, J. Hyper. Differential Equations **12** (2015), 87–188.
16. James Isenberg and Vincent Moncrief, *Asymptotic behavior of the gravitational field and the nature of singularities in Gowdy spacetimes*, Annals of Physics **199** (1990), no. 1, 84–122, DOI: [10.1016/0003-4916\(90\)90369-Y](https://doi.org/10.1016/0003-4916(90)90369-Y).
17. S. Kichenassamy and A. D. Rendall, *Analytic description of singularities in Gowdy spacetimes*, Class. Quantum Grav. **15** (1998), no. 5, 1339–1355.
18. P.G. LeFloch and A.D. Rendall, *A global foliation of Einstein–Euler spacetimes with Gowdy-symmetry on T^3* , Arch. Rat. Mech. **201** (2011), no. 3, 841–870.
19. P.G. LeFloch and Changhua Wei, *The nonlinear stability of self-gravitating irrotational Chaplygin fluids in a FLRW geometry*, Annales de l’Institut Henri Poincaré C, Analyse non linéaire **38** (2021), 757–814.
20. C. Liu and T.A. Oliynyk, *Cosmological Newtonian limits on large spacetime scales*, Commun. Math. Phys. **364** (2018), 1195–1304.
21. ———, *Newtonian limits of isolated cosmological systems on long time scales*, Annales Henri Poincaré **19** (2018), 2157–2243.
22. C. Liu and C. Wei, *Future stability of the FLRW spacetime for a large class of perfect fluids*, Ann. Henri Poincaré **22** (2021), 715–779.
23. C. Lübbe and J. A. Valiente Kroon, *A conformal approach for the analysis of the non-linear stability of radiation cosmologies*, Annals of Physics **328** (2013), 1–25.
24. E. Marshall and T.A. Oliynyk, *On the stability of relativistic perfect fluids with linear equations of state $p = K\rho$ where $1/3 < K < 1$* , arXiv preprint arXiv:2209.06982 (2022).
25. Viatcheslav F Mukhanov, *Physical foundations of cosmology*, Cambridge University Press, 2005.
26. T. A. Oliynyk, *Future stability of the FLRW fluid solutions in the presence of a positive cosmological constant*, Commun. Math. Phys. **346** (2016), 293–312; see the preprint [arXiv:1505.00857] for a corrected version.
27. T.A. Oliynyk, *The cosmological Newtonian limit on cosmological scales*, Commun. Math. Phys. **339** (2015), 455–512.
28. ———, *Future global stability for relativistic perfect fluids with linear equations of state $p = K\rho$ where $1/3 < K < 1/2$* , SIAM J. Math. Anal. **53** (2021), 4118–4141.
29. A. D. Rendall, *Fuchsian analysis of singularities in Gowdy spacetimes beyond analyticity*, Class. Quantum Grav. **17** (2000), no. 16, 3305–3316.
30. A. D. Rendall, *Asymptotics of solutions of the Einstein equations with positive cosmological constant*, Ann. Henri Poincaré **5** (2004), no. 6, 1041–1064.

31. H. Ringström, *Power Law Inflation*, Commun. Math. Phys. **290** (2009), no. 1, 155–218.
32. H. Ringström, *Strong cosmic censorship in T^3 -Gowdy spacetimes*, Ann. Math. **170** (2009), no. 3, 1181–1240.
33. I. Rodnianski and J. Speck, *The stability of the irrotational Euler-Einstein system with a positive cosmological constant*, J. Eur. Math. Soc. **15** (2013), 2369–2462.
34. K. Schneider, D. Kolomenskiy, and E. Deriaz, *Is the CFL condition sufficient? Some remarks*, The Courant-Friedrichs-Lewy (CFL) Condition - 80 Years after its discovery (Unknown, Unknown Region) (C. A. De Moura and C. S. Kubrusly, eds.), 2013, pp. 139–146.
35. J. Speck, *The nonlinear future-stability of the FLRW family of solutions to the Euler-Einstein system with a positive cosmological constant*, Selecta Mathematica **18** (2012), 633–715.
36. ———, *The stabilizing effect of spacetime expansion on relativistic fluids with sharp results for the radiation equation of state*, Arch. Rat. Mech. **210** (2013), 535–579.
37. C. Wei, *Stabilizing effect of the power law inflation on isentropic relativistic fluids*, Journal of Differential Equations **265** (2018), 3441 – 3463.

DEPT OF MATHEMATICS AND STATISTICS, 730 CUMBERLAND ST, UNIVERSITY OF OTAGO, DUNEDIN 9016, NEW ZEALAND
Email address: fbeyer@maths.otago.ac.nz

SCHOOL OF MATHEMATICS, 9 RAINFOREST WALK, MONASH UNIVERSITY, VIC 3800, AUSTRALIA
Email address: elliot.marshall@monash.edu

SCHOOL OF MATHEMATICS, 9 RAINFOREST WALK, MONASH UNIVERSITY, VIC 3800, AUSTRALIA
Email address: todd.oliynyk@monash.edu